J|A|C|S
ARTICLES
Published on Web 10/10/2007

Versatility of the Electronic Structure of Compound I in Catalase-Peroxidases

Pietro Vidossich,[†] Mercedes Alfonso-Prieto,[†] Xavi Carpena,[‡] Peter C. Loewen,[§] Ignacio Fita,[‡] and Carme Rovira*,[†,||]

Contribution from the Centre de Recerca en Química Teòrica, Parc Científic de Barcelona, Josep Samitier 1-5, 08028 Barcelona, Spain, Institut de Biologia Molecular (IBMB-CSIC), Institut de Recerca Biomèdica (IRB), Parc Científic de Barcelona, Josep Samitier 1-5, 08028 Barcelona, Spain, Department of Microbiology, University of Manitoba, Winnipeg MB R3T 2N2, Canada, Institució Catalana de Recerca i Estudis Avançats (ICREA), Passeig Lluís Companys, 23, 08018 Barcelona, Spain

Received March 30, 2007; E-mail: crovira@pcb.ub.es

Abstract: Catalase-peroxidases (KatGs) are bifunctional heme proteins, belonging to the family of class I peroxidases, that are able to catalyze both catalatic and peroxidatic reactions within a peroxidase-like structure. We investigated the electronic structure of reaction intermediates of the catalytic cycle of KatGs by means of density functional theory (DFT) QM/MM calculations. The outcome was that the ionization state of the KatG-specific covalent adduct (Met264-Tyr238-Trp111) affects the radical character of compound I (Cpd I). Specifically, in the optimized structures, substantial radical character is observed on the proximal Trp330 when Tyr238 is protonated, whereas when Tyr238 is deprotonated the radical localizes on the Met^{+}-Tyr(O^{-})-Trp adduct. These findings are not affected by protein thermal fluctuations, although details of the spin density distribution are affected by the geometry of the active site. Calculations provide structures in good agreement with the crystal structure of BpKatG Cpd I. They also provide an explanation for the experimental findings of the mobile and catalatic-specific residue Arg426 being 100% in conformation R in the X-ray structure of BpKatG treated with organic peroxides. The role of different Cpd I forms in the catalase and peroxidase reaction pathways is discussed.

1. Introduction

Catalase-peroxidases (KatGs) are bifunctional heme proteins belonging to class I of the peroxidase superfamily (plants, fungi, and bacteria).[1] Recent work has shown that some examples of the enzyme also have associated NADH oxidase, INH lyase, and isonicotinoyl-NAD synthase activities.[2] The latter two activities are responsible for the activation of isoniazid as an antitubercular drug in *Mycobacterium tuberculosis*,[3] a cause for considerable interest in the enzyme.[4]

The catalase and peroxidase reactions both involve compound I (Cpd I) formation (reaction 1), with the heme initially oxidized to the oxoferryl state (Fe^{IV}=O) and a second oxidizing equivalent stored on the porphyrin ($Por^{\bullet+}$)[5] or on a protein residue after electron transfer (reaction 2).[6−8] Recent works have shown that in this case the oxoferryl oxygen is protonated.[9−11] It is in the reduction of Cpd I back to the resting state that the catalase and peroxidase reactions differ. In the catalatic reaction, Cpd I is reduced in a single two-electron transfer from H_2O_2 (reaction 3), whereas in the peroxidatic reaction Cpd I undergoes two sequential one-electron transfers, usually from organic donors, and involves an intermediate called compound II (Cpd II, reactions 4 and 5).[12]

$$\text{Enz (Por}-\text{Fe}^{\text{III}}) + \text{H}_2\text{O}_2 \rightarrow \text{Cpd I (Por}^{\bullet+}-\text{Fe}^{\text{IV}}=\text{O}) + \text{H}_2\text{O} \quad (1)$$

$$\text{Cpd I (Por}^{\bullet+}-\text{Fe}^{\text{IV}}=\text{O}) \rightarrow \text{Cpd I* (Por}-\text{Fe}^{\text{IV}}-\text{OH, aa}^{+\bullet}) \quad (2)$$

$$\text{Cpd I (Por}^{\bullet+}-\text{Fe}^{\text{IV}}=\text{O}) + \text{H}_2\text{O}_2 \rightarrow \text{Enz (Por}-\text{Fe}^{\text{III}}) + \text{H}_2\text{O} + \text{O}_2 \quad (3)$$

$$\text{Cpd I} + \text{H}^{+} + \text{A}_{\text{red}} \rightarrow \text{Cpd II (Por}-\text{Fe}^{\text{IV}}-\text{OH}) + \text{A}_{\text{ox}} \quad (4)$$

$$\text{Cpd II (Por}-\text{Fe}^{\text{IV}}-\text{OH}) + \text{H}^{+} + \text{A}_{\text{red}} \rightarrow \text{Enz (Por}-\text{Fe}^{\text{III}}) + \text{H}_2\text{O} + \text{A}_{\text{ox}} \quad (5)$$

There are several differences in the reaction kinetics between KatGs and monofunctional enzymes. Monofunctional catalases and peroxidases exhibit faster kinetics and are active over a

[†] Centre de Recerca en Química Teòrica, Parc Científic de Barcelona.
[‡] Institut de Biologia Molecular (IBMB-CSIC), Institut de Recerca Biomèdica (IRB), Parc Científic de Barcelona.
[§] University of Manitoba.
[||] Institució Catalana de Recerca i Estudis Avançats (ICREA).

(1) Klotz, M. G.; Loewen, P. C. *Mol. Biol. Evol.* **2003**, *20*, 1098−1112.
(2) Singh, R.; Wiseman, B.; Deemagarn, T.; Donald, L. J.; Duckworth, H. W.; Carpena, X.; Fita, I.; Loewen, P. C. *J. Biol. Chem.* **2004**, *279*, 43098−43106.
(3) Deretic, V.; PaganRamos, E.; Zhang, Y. Q.; Dhandayuthapani, S.; Via, L. E. *Nat. Biotechnol.* **1996**, *14*, 1557−1561.
(4) Wei, C. J.; Lei, B. F.; Musser, J. M.; Tu, S. C. *Antimicrob. Agents Chemother.* **2003**, *47*, 670−675.
(5) Ivancich, A.; Jouve, H. M.; Sartor, B.; Gaillard, J. *Biochemistry* **1997**, *36*, 9356−9364.
(6) Hillar, A.; Nicholls, P.; Switala, J.; Loewen, P. C. *Biochem. J.* **1994**, *300*, 531−539.

10.1021/ja072245i CCC: $37.00

broad pH range,[8,12,13] whereas KatG activities are restricted to relatively narrow pH ranges that differ for the catalase and peroxidase activities.[2] The maximum peroxidase activity takes place at acidic pH (pH ≈ 4.5 in *Burkholderia pseudomallei*, BpKatG) while the maximum catalase activity occurs at more basic values (pH ≈ 6.5 in BpKatG).[2] Until recently, it was commonly assumed that the catalatic mechanism of KatGs was similar to that of monofunctional catalases. However, recent stop-flow spectroscopy studies of KatGs revealed spectral characteristics not previously noted in monofunctional catalases, suggesting a different catalatic reaction pathway.[14−17]

Detailed structural information of KatGs is available from the crystal structures of the enzymes from *Haloarcula marismortui*, HmKatG;[18,19] *Burkholderia pseudomallei*, BpKatG;[20] *Synechococcus*, PCC7942;[21] and *Mycobacterium tuberculosis*, MtKatG.[22] These structures revealed the similarity between the active sites of KatGs and (class I) peroxidases, such as cytochrome c peroxidase (CcP) and ascorbate peroxidase (APX).[23,24] Biochemical characterization of variants of KatGs from different sources led to the identification of a number of peroxidase- and catalase-specific residues (reviewed in ref 25). The Arg108/Trp111/His112 triad on the distal side and the His279/Asp389/Trp330 triad on the proximal side (see Figure 1; all numbering is for BpKatG unless otherwise stated) are characteristic of class I peroxidases.[12] To impart catalase activity to the peroxidase core, Asp141 and a cross-linked adduct formed by Trp111, Tyr238, and Met264 (hereafter the Met^{+}-Tyr-Trp adduct) and Arg426 are required. Asp141 is believed to control the entry of substrate into the active site,[26] but the precise role of the adduct and Arg426 remains unclear.[14,15,27−29]

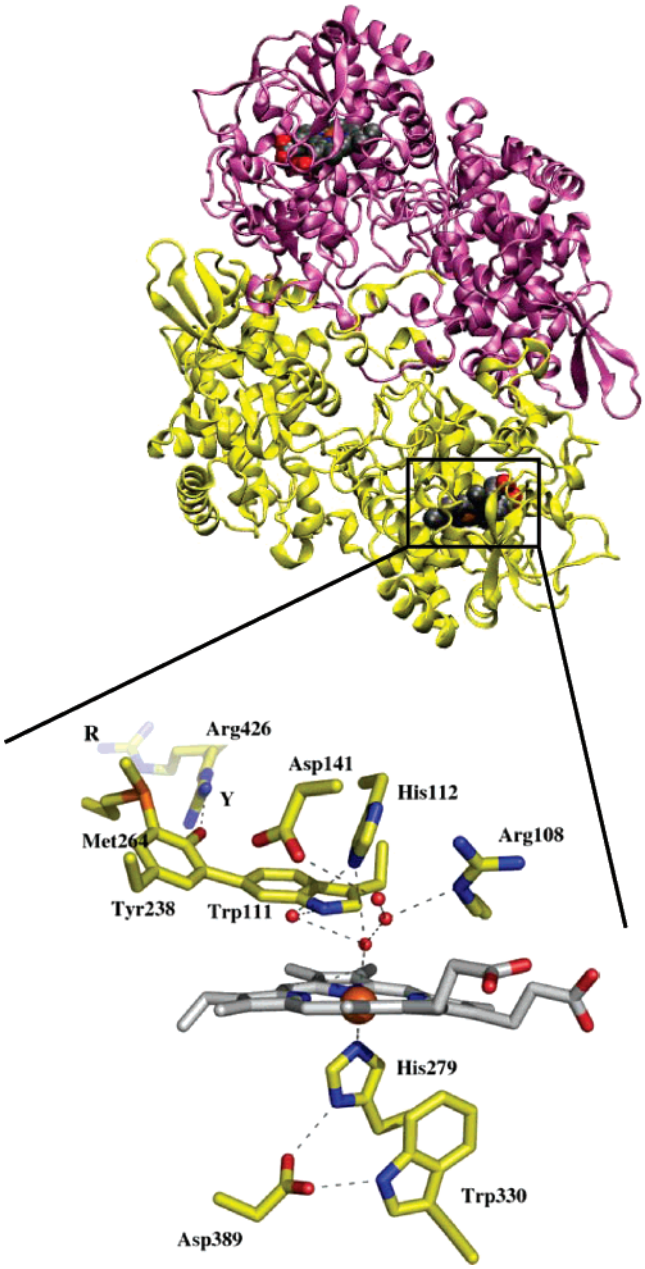

Figure 1. Structure of native BpKatG (PDB entry 1MWV). (Top) Cartoon picture of the protein, with one subunit colored in yellow, the other in pink, and the heme prosthetic groups in gray. (Bottom) Heme binding pocket. Both *R* and *Y* conformations of Arg426 are displayed.

The unusual Met^{+}-Tyr-Trp adduct has been observed in all KatG structures, and mass spectrometry studies have confirmed its presence.[27,28] Moreover, mutation of any of the three residues constituting the adduct impair the catalatic activity with limited effects upon the peroxidatic activity.[25] To our knowledge, the Met^{+}-Tyr-Trp adduct is unique to KatGs. Modified tyrosines have been observed in the active site of galactose oxidase,[30] catalase-1 from *Neurospora crassa*[31] (Tyr-Cys thioether bond), catalase HPII from *Escherichia coli* (Tyr-His),[32] and cytochrome

(7) Ivancich, A.; Jakopitsch, C.; Auer, M.; Un, S.; Obinger, C. *J. Am. Chem. Soc.* **2003**, *125*, 14093−14102.
(8) Zamocky, M.; Koller, F. *Prog. Biophys. Mol. Biol.* **1999**, *72*, 19−66.
(9) Alfonso-Prieto, M.; Borovik, A.; Carpena, X.; Murshudov, G.; Melik-Adamyan, W.; Fita, I.; Rovira, C.; Loewen, P. C. *J. Am. Chem. Soc.* **2007**, *129*, 4193−4205.
(10) Hersleth, H. P.; Ryde, U.; Rydberg, P.; Gorbitz, C. H.; Andersson, K. K. *J. Inorg. Biochem.* **2006**, *100*, 460−476.
(11) Rovira, C. *ChemPhysChem* **2005**, *6*, 1820−1826.
(12) Dunford, H. B. *Heme Peroxidases*; Wiley-VCH: New York, 1999.
(13) Nichols, P.; Fita, I.; Loewen, P. C. Enzymology and Structure of Catalases. In *Advances in Inorganic Chemistry*; Sykes, A. G., Mauk, G., Eds.; Academic Press: 2001; pp 51−106.
(14) Ghiladi, R. A.; Knudsen, G. M.; Medzihradszky, K. F.; de Montellano, P. R. O. *J. Biol. Chem.* **2005**, *280*, 22651−22663.
(15) Jakopitsch, C.; Ivancich, A.; Schmuckenschlager, F.; Wanasinghe, A.; Poltl, G.; Furtmuller, P. G.; Ruker, F.; Obinger, C. *J. Biol. Chem.* **2004**, *279*, 46082−46095.
(16) Jakopitsch, C.; Wanasinghe, A.; Jantschko, W.; Furtmuller, P. G.; Obinger, C. *J. Biol. Chem.* **2005**, *280*, 9037−9042.
(17) Jakopitsch, C.; Vlasits, J.; Wiseman, B.; Loewen, P. C.; Obinger, C. *Biochemistry* **2007**, *46*, 1183−1193.
(18) Yamada, Y.; Fujiwara, T.; Sato, T.; Igarashi, N.; Tanaka, N. *Nat. Struct. Biol.* **2002**, *9*, 691−695.
(19) Yamada, Y.; Saijo, S.; Sato, T.; Igarashi, N.; Usui, H.; Fujiwara, T.; Tanaka, N. *Acta Crystallogr., Sect. D* **2001**, *57*, 1157−1158.
(20) Carpena, X.; Loprasert, S.; Mongkolsuk, S.; Switala, J.; Loewen, P. C.; Fita, I. *J. Mol. Biol.* **2003**, *327*, 475−489.
(21) Wada, K.; Tada, T.; Nakamura, Y.; Kinoshita, T.; Tamoi, M.; Shigeoka, S.; Nishimura, K. *Acta Crystallogr., Sect. D* **2002**, *58*, 157−159.
(22) Bertrand, T.; Eady, N. A. J.; Jones, J. N.; Nagy, J. M.; Jamart-Gregoire, B.; Raven, E. L.; Brown, K. A. *J. Biol. Chem.* **2004**, *279*, 38991−38999.
(23) Barrows, T. P.; Poulos, T. L. *Biochemistry* **2005**, *44*, 14062−14068.
(24) Welinder, K. G. *Curr. Opin. Struct. Biol.* **1992**, *2*, 388−393.
(25) Smulevich, G.; Jakopitsch, C.; Droghetti, E.; Obinger, C. *J. Inorg. Biochem.* **2006**, *100*, 568−585.
(26) Deemagarn, T.; Wiseman, B.; Carpena, X.; Ivancich, A.; Fita, I.; Loewen, P. C. *Proteins* **2007**, *66*, 219−228.
(27) Donald, L. J.; Krokhin, O. V.; Duckworth, H. W.; Wiseman, B.; Deemagarn, T.; Singh, R.; Switala, J.; Carpena, X.; Fita, I.; Loewen, P. C. *J. Biol. Chem.* **2003**, *278*, 35687−35692.
(28) Jakopitsch, C.; Kolarich, D.; Petutschnig, G.; Furtmuller, P. G.; Obinger, C. *FEBS Lett.* **2003**, *552*, 135−140.
(29) Jakopitsch, C.; Auer, M.; Ivancich, A.; Ruker, F.; Furtmuller, P. G.; Obinger, C. *J. Biol. Chem.* **2003**, *278*, 20185−20191.
(30) Ito, N.; Phillips, S. E. V.; Stevens, C.; Ogel, Z. B.; Mcpherson, M. J.; Keen, J. N.; Yadav, K. D. S.; Knowles, P. F. *Nature* **1991**, *350*, 87−90.
(31) Diaz, A.; Horjales, E.; Rudino-Pinera, E.; Arreola, R.; Hansberg, W. *J. Mol. Biol.* **2004**, *342*, 971−985.
(32) Melik-Adamyan, W.; Bravo, J.; Carpena, X.; Switala, J.; Mate, M. J.; Fita, I.; Loewen, P. C. *Proteins* **2001**, *44*, 270−281.

c oxidase[33,34] (Tyr-His), and it has been proposed that these enzymes exploit the modified properties (oxidation potential, acidity, and bond strength) of the crosslinked species for catalysis.[35] No examples of Met-Tyr side-chain cross-links have been reported to date, while the only example of a Trp-Tyr bond comes from a CcP mutant[36] (H52Y, but note that here a C−N bond is formed, as opposed to the C−C bond in KatGs).

The role of Arg426 is particularly enigmatic because it is not in direct contact with the heme (the C_α is almost 20 Å away from the iron of the porphyrin), and yet it enhances the catalase reaction 10-fold.[25,37] The side chain of Arg426 can adopt two conformations (Figure 1). In one position, it forms a close association with Tyr238 in the Met^+-Tyr-Trp adduct (conformation *Y*), and in the second position, it is shifted away from the adduct to a region containing two other arginine residues (conformation *R*). The relative proportion of *Y* and *R* conformers is pH dependent, and a systematic study of changes occurring in the structure of BpKatG as the pH of crystals is varied across the pH range from 4.5 to 8.5 revealed a change from >90% *R* : < 10% *Y* at pH 4.5 (the optimum pH for the peroxidatic activity) to <5% *R* : > 95% *Y* at pH 8.5.[38] The relative proportion at pH 6.5 (the optimum pH for the catalatic activity) is 50% *R* : 50% *Y*.

The pH dependence of the Arg426 side-chain conformation coupled with its key role in catalase activity suggested that it can act as a molecular switch reversibly interacting with the Met^+-Tyr-Trp adduct to inductively alter heme reactivity.[37] As both the catalatic and peroxidatic pathways involve the formation of Cpd I (reaction 1), the role of Arg426 most logically lies in the reduction of Cpd I (reaction 3). However, the structure of BpKatG Cpd I has Arg426 100% in conformation *R* both at mild acidic and basic conditions.[37] Such a significant change in the *R:Y* equilibrium occurring upon Cpd I formation followed by its reversal during Cpd I reduction suggests a very dynamic catalytic process sensitive to the protonation state of the adduct. Interestingly, recent spectroscopic investigations of the reaction of KatG with H_2O_2 detected two different species, depending on the pH,[17] with the transition among the two in the pH range 6−7, depending on the source of KatG.[17] The spectrum of the high-pH species (at pH 8.5 exhibited maxima at 418 and 520 nm) did not resemble the spectrum of any reaction intermediate previously reported in peroxidases or catalases. The spectrum of the low-pH species (at pH 5.6, exhibited maxima at 415, 545, and 580 nm) resembled the spectra of other intermediates or complexes observed in peroxidase chemistry (see ref 17 for a full discussion). This study suggests that either the catalatic reaction follows different pathways, depending on the pH, or that the rate-limiting step varies, depending on the pH. It is the objective of the present study to investigate the pH dependence of the electronic structure of the reaction intermediates Cpd I and Cpd II. Among the titratable residues within the active site, His112 and Asp141 can be ruled out as responsible for the pH-dependent behavior. His112 is supposed to display a pK_a < 5.5,[39] although smaller values have been proposed.[12] Asp141 is solvent exposed and not in direct contact with any charged residue; thus, its pK_a is expected to be ∼4. Tyr238 forms in the resting enzyme a pH-sensitive ionic bond with Arg426, and an apparent pK_a of 6.5 may be inferred from crystallographic studies.[37,38] Therefore, the effect of the different protonation states of Tyr238 and its different association states with Arg426 could be responsible for the observed pH changes.

In an attempt to solve these issues, theoretical techniques could be very useful to complement experimental studies. In recent years, several density functional theory (DFT) studies of reaction intermediates of monofunctional catalases[11,40−42] and peroxidases have appeared, including HRP,[43−45] CcP,[46] APX,[46] and cytP450[43,47] as well as more general analyses.[48−52] These studies show that DFT is suitable for the description of the electronic structure of these complex active sites. Recent DFT QM/MM studies on HRP disentangled the complex electronic structures of HRP Cpds I and II and showed that the electronic properties of the reaction intermediates are modulated by the protein environment.[44,45] Similar studies have also been performed for other heme proteins.[10] To the best of our knowledge, the reaction intermediates of KatGs have not yet been studied by DFT or other quantum chemistry methods.

In this report, we investigate the electronic properties of the KatG-specific Met^+-Tyr-Trp adduct and the reaction intermediates of BpKatG by means of DFT and DFT QM/MM techniques. First, we show that the covalent linkage of Met, Tyr, and Trp modifies their redox and ionization properties with respect to the free residues. Second, we show that the radical characters of Cpd I and Cpd II active sites are significantly affected by the protonation state of the adduct and that the classic porphyrin radical of Cpd I preferentially migrates to one of two locations, depending on the pH. We propose that there are several different types of Cpd I present in active KatGs which have similar protein and heme structures but different electronic structures. Finally, the role of these electronically different Cpd I species in the catalase and peroxidase reaction pathways are discussed in the light of the experimental information available.

2. Methods

2.1. Initial Structures. The initial structures for the calculations were built from the X-ray structures of BpKatG Cpd I at pH 5.6 (resolution 1.9 Å, PDB entry 2B2R)[20] and native BpKatG at pH 8.5 (resolution 1.95 Å, PDB entry 2FXJ).[37] The structure of BpKatG Cpd

(33) Ostermeier, C.; Harrenga, A.; Ermler, U.; Michel, H. *Proc. Natl. Acad. Sci. U.S.A.* **1997**, *94*, 10547−10553.
(34) Yoshikawa, S.; Shinzawa-Itoh, K.; Nakashima, R.; Yaono, R.; Yamashita, E.; Inoue, N.; Yao, M.; Fei, M. J.; Libeu, C. P.; Mizushima, T.; Yamaguchi, H.; Tomizaki, T.; Tsukihara, T. *Science* **1998**, *280*, 1723−1729.
(35) Himo, F.; Siegbahn, P. E. M. *Chem. Rev.* **2003**, *103*, 2421−2456.
(36) Bhaskar, B.; Immoos, C. E.; Shimizu, H.; Sulc, F.; Farmer, P. J.; Poulos, T. L. *J. Mol. Biol.* **2003**, *328*, 157−166.
(37) Carpena, X.; Wiseman, B.; Deemagarn, T.; Singh, R.; Switala, J.; Ivancich, A.; Fita, I.; Loewen, P. C. *EMBO Rep.* **2005**, *6*, 1156−1162.
(38) Carpena, X.; Wiseman, B.; Deemagarn, T.; Herguedas, B.; Ivancich, A.; Singh, R.; Loewen, P. C.; Fita, I. *Biochemistry* **2006**, *45*, 5171−5179.
(39) Hashimoto, S.; Tatsuno, Y.; Kitagawa, T. *Proc. Natl. Acad. Sci. U.S.A.* **1986**, *83*, 2417−2421.
(40) de Visser, S. P. *Inorg. Chem.* **2006**, *45*, 9551−9557.
(41) Horner, O.; Oddou, J. L.; Mouesea, J. M.; Jouve, H. M. *J. Inorg. Biochem.* **2006**, *100*, 477−479.
(42) Horner, O.; Mouesca, J. M.; Solari, P. L.; Orio, M.; Oddou, J. L.; Bonville, P.; Jouve, H. M. *J. Biol. Inorg. Chem.* **2007**, *12*, 509−525.
(43) de Visser, S. P.; Shaik, S.; Sharma, P. K.; Kumar, D.; Thiel, W. *J. Am. Chem. Soc.* **2003**, *125*, 15779−15788.
(44) Derat, E.; Cohen, S.; Shaik, S.; Altun, A.; Thiel, W. *J. Am. Chem. Soc.* **2005**, *127*, 13611−13621.
(45) Derat, E.; Shaik, S. *J. Am. Chem. Soc.* **2006**, *128*, 8185−8198.
(46) Bathelt, C. M.; Mulholland, A. J.; Harvey, J. N. *Dalton Trans.* **2005**, 3470−3476.
(47) Guallar, V.; Baik, M. H.; Lippard, S. J.; Friesner, R. A. *Proc. Natl. Acad. Sci. U.S.A.* **2003**, *100*, 6998−7002.
(48) Bassan, A.; Blomberg, M. R. A.; Borowski, T.; Siegbahn, P. E. M. *J. Inorg. Biochem.* **2006**, *100*, 727−743.
(49) Behan, R. K.; Green, M. T. *J. Inorg. Biochem.* **2006**, *100*, 448−459.
(50) Green, M. T. *J. Am. Chem. Soc.* **2006**, *128*, 1902−1906.
(51) Kuramochi, H.; Noodleman, L.; Case, D. A. *J. Am. Chem. Soc.* **1997**, *119*, 11442−11451.
(52) Silaghi-Dumitrescu, R. *J. Biol. Inorg. Chem.* **2004**, *9*, 471−476.

I was used as a model for the *R* conformation of Arg426, while the native BpKatG at pH 8.5 was used as a model for the *Y* conformation. Hydrogen atoms were added using standard bond lengths and bond angles. The protein was solvated with water molecules (38531 and 42393 water molecules for Arg426 in *R* and *Y* conformations, respectively), and Na^+ ions were added to neutralize the simulation cell. All Arg, Lys, Asp, and Glu residues were considered in their ionized form. The protonation state of the histidine residues took into account their hydrogen bond environment. For each subunit, histidines 53, 55, 85, 101, 285, 339, 360, 381, 406, 455, 568, and 650 were considered diprotonated, His112, His279, and His425 were considered N_δ-protonated, and His709 was taken as N_ε-protonated.

2.2. DFT Calculations. Gas-phase quantum chemical calculations were performed to investigate the properties of the covalent adduct. A model of the isolated Met^+-Tyr-Trp covalent adduct and that of the Met^+-Tyr-Trp:Arg426 complex were constructed from the X-ray structure of native BpKatG at pH 8.5.[37] The structures were optimized within the spin-unrestricted DFT framework,[53,54] using the Car−Parrinello molecular dynamics (CPMD) program.[55] Valence orbitals were expanded with a plane wave basis set up to 70 Ry. Martins−Troullier pseudopotentials[56] were used to describe the core electron-valence shell electron interactions. The Becke and Perdew functionals (BP86) were used for exchange and correlation interactions, respectively.[57,58] This functional form has been previously used by several groups in DFT studies on metal-based bioinorganic systems.[9,11,41,42,51,59−61] Geometry optimizations were performed using the DIIS method[62] until the largest component of the nuclear gradient was lower than 5×10^{-4} au.

Deprotonation energies (deprE) were calculated as the difference between the energy of the protonated [Met^+-Tyr(OH)-Trp(NH)] and deprotonated adduct [Met^+-Tyr(O^-)-Trp(NH) or Met^+-Tyr(OH)-Trp-(N^-), depending whether deprotonation takes place at Tyr or Trp], both at the equilibrium geometry. Ionization potentials (IPs) were calculated as the difference between the energy of the adduct radical and the closed-shell system, both at the equilibrium geometry. Different configurations of the adduct were considered, depending on the protonation state of the adduct (only protonation at Tyr was considered) and whether it interacts with Arg426.

2.3. pK_a and Binding Energy Calculations. Additional calculations have been performed to calculate the free energy of binding of the Met^+-Tyr-Trp:Arg426 interaction and the pK_a of the Met^+-Tyr-Trp adduct. Calculations follow standard procedures[63−65] and are described in the Supporting Information (SI).

2.4. Molecular Dynamics Simulations. Classical molecular dynamics (MD) simulations were performed in order to equilibrate the protein frame and to address the effects of thermal fluctuations on the active-site electronic structure. The approach used here exploits the efficiency of classical MD to sample protein conformation in the multi-nanosecond time scale coupled to the calculation of the active-site electronic structure at the QM/MM level for selected snapshots along the MD trajectory. All computational details concerning the classical MD simulations are collected in the Supporting Information.

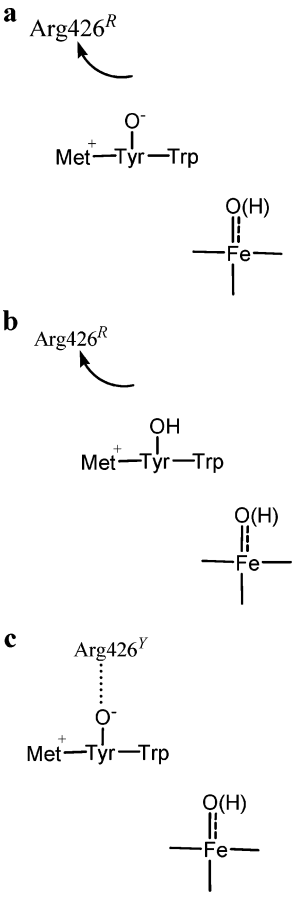

Figure 2. Active-site configurations used in the calcualtions. (a) Arg426 is in the *R* position and Tyr238 is unprotonated. (b) Arg426 is in the *R* position and Tyr238 is protonated. (c) Arg426 is in the *Y* position and Tyr238 is unprotonated.

Table 1. Models Used in the QM/MM Calculations

model	adduct protonation state	Arg426 conformation	spin state
Ia	Met^+-Tyr(O^-)-Trp	*R*	quartet
Ib	Met^+-Tyr(OH)-Trp	*R*	quartet
Ic	Met^+-Tyr(O^-)-Trp	*Y*	quartet
IIa	Met^+-Tyr(O^-)-Trp	*R*	triplet
IIb	Met^+-Tyr(OH)-Trp	*R*	triplet

2.5. Hybrid DFT QM/MM Calculations. Three different configurations were considered (Figure 2 and Table 1). Models **a** and **b** have Arg426 in the *R* position (i.e., not interacting with the adduct) and include in the QM region the side chains of residues Arg108, Trp111, His112, Asp141, Tyr238, Met264, His279, Trp330, Asp389, and the heme group, excluding the propionates (i.e., we considered them as part of the MM region). The difference between **a** and **b** is only the protonation state of the adduct Tyr238 (unprotonated in **a** and protonated in **b**). Both models are compatible with the crystal structure of BpKatG Cpd I[37] (Arg426^R, where the protonation state of the adduct cannot be inferred). Model **c** differs from the previous ones in the position of Arg426 (Arg426^Y, now included in the QM region), where the adduct can only be unprotonated. Even though this configuration is not compatible with the crystal structure of Cpd I,[37] it is interesting to characterize the differences observed in terms of electronic structure.

We will refer to the systems in which the QM region is two oxidizing equivalents above the resting state as Cpd I (or I). These systems were

(53) Hohenberg, P. K. W. *Phys. Rev. B: Condens. Mater. Phys.* **1964**, *136*, 864−871.
(54) Kohn, W.; Sham, L. J. *Phys. Rev. A: At., Mol., Opt. Phys.* **1965**, *140*, 1133−1138.
(55) *CPMD 3.10*; MPI für Festkörperforschung Stuttgart and IBM Zurich Research Laboratory, 2006.
(56) Troullier, N.; Martins, J. L. *Phys. Rev. B: Condens. Mater. Phys.* **1991**, *43*, 1943−2006.
(57) Becke, A. D. *J. Chem. Phys.* **1986**, *84*, 4524−4529.
(58) Perdew, J. P. *Phys. Rev. B: Condens. Mater. Phys.* **1986**, *33*, 8822−8824.
(59) Kuta, J.; Patchkovskii, S.; Zgierski, M. Z.; Kozlowski, P. M. *J. Comput. Chem.* **2006**, *27*, 1429−1437.
(60) Nilsson, K.; Hersleth, H. P.; Rod, T. H.; Andersson, K. K.; Ryde, U. *Biophys. J.* **2004**, *87*, 3437−3447.
(61) Rovira, C.; Kozlowski, P. M. *J. Phys. Chem. B* **2007**, *111*, 3251−3257.
(62) Csaszar, P.; Pulay, P. *J. Mol. Struct.* **1984**, *114*, 31−34.
(63) Himo, F.; Noodleman, L.; Blomberg, M. R. A.; Siegbahn, P. E. M. *J. Phys. Chem. A* **2002**, *106*, 8757−8761.
(64) Ullmann, G. M.; Noodleman, L.; Case, D. A. *J. Biol. Inorg. Chem.* **2002**, *7*, 632−639.
(65) Klicic, J. J.; Friesner, R. A.; Liu, S. Y.; Guida, W. C. *J. Phys. Chem. A* **2002**, *106*, 1327−1335.

computed in a quartet spin state ($S = {}^3/_2$) and doublet spin states ($S = {}^1/_2$). In agreement with previous theoretical studies of class I and class III peroxidases[44,46] and catalases,[9,40] we found that the quartet is slightly lower in energy and the two show a similar spin distribution (see Table 3S). We performed separate calculations, considering either an oxoferryl (Fe═O) or hydroxoferryl (Fe−OH) moieties. It is important to stress the fact that in our calculations there is no restriction on the distribution of the unpaired electrons within the QM region. Therefore, the third unpaired electron is not forced to be on the porphyrin.

The systems in which the active site is one oxidizing equivalent above the resting state will be referred as Cpd II (or II). In this case the calculations were done in the triplet state ($S = 1$), which turned to be the lowest-energy spin state, as found in monofunctional peroxidases[45] and catalases (the singlet and quintuplet states were found to be higher in energy).[9,11] The oxoferryl unit of Cpd II was taken as protonated since it is generally assumed that Cpd II is protonated at neutral pH.[11,41,60]

In order to assess the influence of different residues on the electronic structure of the reaction intermediates, additional calculations were performed considering different QM/MM partitions. All models are described in the Supporting Information (see Scheme 1S).

The QM/MM calculations were performed within a fully Hamiltonian coupling scheme between the QM region (the active site, as described above) and the classical regions (the rest of the protein in aqueous solution, in the presence of counterions).[66] Dangling bonds were saturated by hydrogen atoms. Spurious electrostatic interactions between the capping hydrogens and close-by classical atoms were excluded from the QM/MM Hamiltonian according to ref 67. Electrostatic interactions were taken into account within a multilayer approach.[67,68] Bonded and van der Waals interactions between the QM and MM parts, as well as within the MM region, were accounted for by the AMBER force field.[69] In all QM calculations the QM subsystems have been placed in a supercell and treated as isolated. Calculations were performed with the CPMD code,[55] using a modified version of the GROMOS96 code to compute the MM interactions.[70] Previous work has demonstrated the reliability of the QM/MM CPMD method in the description of structural, energetic, and dynamic properties of systems of biological interest, including hemeproteins (see for instance refs 71−73). Structure optimizations were performed by Car−Parrinello molecular dynamics[74] with annealing of the atomic velocities, using a time step of 5 au and a fictitious electron mass of 850 au to solve the equations of motion. The spin-density distributions have been analyzed in the framework of the atoms in molecules theory.[75] Accordingly, the electron density was written to a grid of spacing ~0.2 Å, and the atomic basins were calculated from it according to the method described in ref 76. The spin density was integrated within these basins.

3. Results

3.1. The Met-Tyr-Trp Adduct. Tables 2, 3, and 4 show the computed properties (deprotonation energies, deprE, pK_a, and ionization potential, IP) of the adduct, in comparison with normal Tyr and Trp residues (modeled by phenol and indole, respectively). It is apparent that the adduct displays altered redox and ionization properties with respect to standard Tyr and Trp amino acids. For instance, the deprotonation energies of the adduct are lower than those in normal Tyr and Trp residues (from 355 to 293 kcal/mol for Trp and from 352 to 260 kcal/mol for Tyr). This is probably due to the presence of the positively charged Met, which stabilizes the anionic form, and the possibility of delocalization of the negative charge onto a more extended π system. Comparing both Tyr and Trp residues, it becomes clear from Table 2 that the hydroxyl group of Tyr is the easiest to deprotonate.

Table 2. Gas-phase Deprotonation Energies (deprE, in kcal/mol) for the Isolated Adduct

process	Arg426	deprE
Met^+-Tyr(OH)-Trp(NH) → Met^+-Tyr(O^-)-Trp(NH)	*R*	260
Met^+-Tyr(OH)-Trp(NH) → Met^+-Tyr(OH)-Trp(N^-)	*R*	293
Met^+-Tyr(O^-)-Trp(NH) → Met^+-Tyr(O^-)-Trp(N^-)	*R*	356
Met^+-Tyr(O^-)-Trp(NH) → Met^+-Tyr(O^-)-Trp(N^-)	*Y*	308
Tyr(OH)-Trp(NH) → Tyr(O^-)-Trp(NH)	−	344
Tyr(OH) → Tyr (O^-)	−	352
Trp(NH) → Trp(N-)	−	355

Table 3. Calculated pK_a's (see Text for Details of the Calculations)

system	pK_a
Met^+-Tyr(OH)-Trp	
in water ($\epsilon = 80$)	7.3
in the protein	7.7
phenol	10.8

Table 4. Gas-Phase Ionization Potentials (IP, in kcal/mol) for the Isolated Adduct

system	IP
Met^+-Tyr(OH)-Trp	218
Met^+-Tyr(O^-)-Trp:Arg426^Y	191
Met^+-Tyr(O^-)-Trp	132
Tyr(OH)-Trp	150
Tyr(O^-)-Trp	50
p-methyl-phenol	181
p-methyl-phenolate	48
3-methyl-indole	167
3-methyl-indolide	50

To estimate the change in the pK_a of the adduct with respect to an unmodified tyrosine residue, solvent effects were calculated, following standard procedures[64,65] (details of the calculations are provided as Supporting Information, section 4S). In view of the lower deprotonation energy of the adduct with respect to a normal Tyr residue, the pK_a of the adduct in water solution is expected to be much lower than that of a normal tyrosine. However, solvation effects act in the opposite direction, with the solvation energy of the protonated adduct, Met^+-TyrOH-Trp, being larger than that of the unprotonated form, Met^+-TyrO^--Trp (the former is positively charged, while the latter is neutral). As a result, the pK_a of the tyrosine in the adduct was determined to be 7.3, about 3 pK_a units lower than an unmodified Tyr.

Within the protein environment, the pK_a of the adduct is only slightly different (pK_a = 7.7) with respect to its value in solution. Indeed, with Arg426 in the R conformation, the adduct is not

(66) Laio, A.; VandeVondele, J.; Roethlisberger, U. *J. Chem. Phys.* **2002**, *116*, 6941.
(67) Laio, A.; Gervasio, F. L.; VandeVondele, J.; Sulpizi, M.; Rothlisberger, U. *J. Phys. Chem. B* **2004**, *108*, 7963−7968.
(68) Laio, A.; VandeVondele, J.; Roethlisberger, U. *J. Phys. Chem. B* **2002**, *106*, 7300−7307.
(69) Cornell, W. D.; Cieplak, P.; Bayly, C. I.; Gould, I. R.; Merz, K. M., Jr.; Ferguson, D. M.; Spellmeyer, D. C.; Fox, T.; Caldwell, J. W.; Kollman, P. A. *J. Am. Chem. Soc.* **1995**, *117*, 5179−5197.
(70) van Gunsteren W. F. *Biomolecular Simulation: The GROMOS96 Manual and User Guide;* Hochschulverlag AG der ETH Zuerich: Zuerich, Groningen, 1996.
(71) Biarnes, X.; Nieto, J.; Planas, A.; Rovira, C. *J. Biol. Chem.* **2006**, *281*, 1432−1441.
(72) Blumberger, J.; Klein, M. L. *J. Am. Chem. Soc.* **2006**, *128*, 13854−13867.
(73) Carloni, P.; Rothlisberger, U.; Parrinello, M. *Acc. Chem. Res.* **2002**, *35*, 455−464.
(74) Car, R.; Parrinello, M. *Phys. Rev. Lett.* **1985**, *55*, 2471−2474.
(75) Bader, R. F. W. *Atoms in Molecules: A Quantum Theory*; Oxford University Press: New York, 1990.
(76) Henkelman, G.; Arnaldsson, A.; Jonsson, H. *Comput. Mater. Sci.* **2006**, *36*, 354−360.

Table 5. Iron−Oxygen Distance (Å) in Cpds I and II

	Fe=O	Fe–OH
Ia	1.71	1.85
Ib	1.71	1.82
Ic	1.70	1.80
IIa	–	1.89
IIb	–	1.84

surrounded by any charged residues that might considerably shift its pK_a. However, the association of the Met$^+$-TyrO$^-$-Trp form with Arg426 is expected to lower the apparent pK_a of the adduct. The binding energy corresponding to this interaction was computed to be −2.2 kcal/mol. To quantify the pK_a change due to the interaction with Arg426, we simulated the relative concentrations of the species at different pHs, taking into account the two coupled reactions (deprotonation of the adduct and its association with Arg426 in the native enzyme, see Supporting Information, section 4S for details). It turned out that equal population of *R* and *Y* conformations of Arg426 occurs at pH 6.1, in fair agreement with the experimental data (50% Arg426^R : 50% Arg426^Y at pH 6.5[38]).

The electron donor ability of the adduct was determined by computing the IP energies for three different situations: protonated adduct, deprotonated adduct, and deprotonated adduct with Arg426 interacting with Tyr238 (Arg426^Y). A lower IP value indicates higher electron-donor ability. As expected, the IP of the protonated adduct [Met$^+$-Tyr(OH) -Trp] is higher (218 kcal/mol) than that of the deprotonated one [Met$^+$-Tyr-(O$^-$)-Trp] (Table 3). For a deprotonated adduct, the IP is higher when Arg426 is close to the adduct (191 kcal/mol) than when it is away from it (132 kcal/mol). The IP of [Met$^+$-Tyr(O$^-$)-Trp] is higher than that of phenolate and indolide, but lower than that of the neutral species, phenol, and indole. Therefore, the IP of the adduct is significantly affected by its protonation state and by the conformation of Arg426. The unprotonated adduct [Met$^+$-Tyr(O$^-$)-Trp] is a better electron donor than the protonated one [Met$^+$-Tyr(OH)-Trp], and its donor ability is reduced when Arg426 is associated with it.

3.2. The Cpd I Active Site. The DFT QM/MM optimized structures of the Cpd I active site are shown in the Supporting Information (Figure 1S). Of particular interest are the Fe−O distances, because recent studies on heme proteins suggest that there is a relation between protonation of the oxoferryl bond and the location of the third unpaired electron in Cpd I.[9,10] In particular, long Fe−O distances are related to migration of the radical from the porphyrin into the protein, while short Fe−O distances (oxoferryl bond) usually correspond to oxoferryl-porphyrin radicals. The Fe−O distances obtained from the calculations are listed in Table 5. The Fe=O (double bond) distances (1.71 Å for both models **Ia** and **Ib**) are the same as those obtained for monofunctional catalases.[9,11] The single bond distances for Cpd I (1.85, 1.82 Å for models **Ia** and **Ib**, respectively) are longer than the distances previously found for monofunctional catalases but in good agreement with the crystal structure of BpKatG Cpd I (Fe−O = 1.88 Å).[37] This suggests that in the crystal structure the oxoferryl bond is protonated and that the third unpaired electron is probably not on the porphyrin.

The spin-density distribution of Cpd I for the three configurations considered is shown in Figure 3. Significantly, the amount of radical character on the porphyrin is rather small, indicating

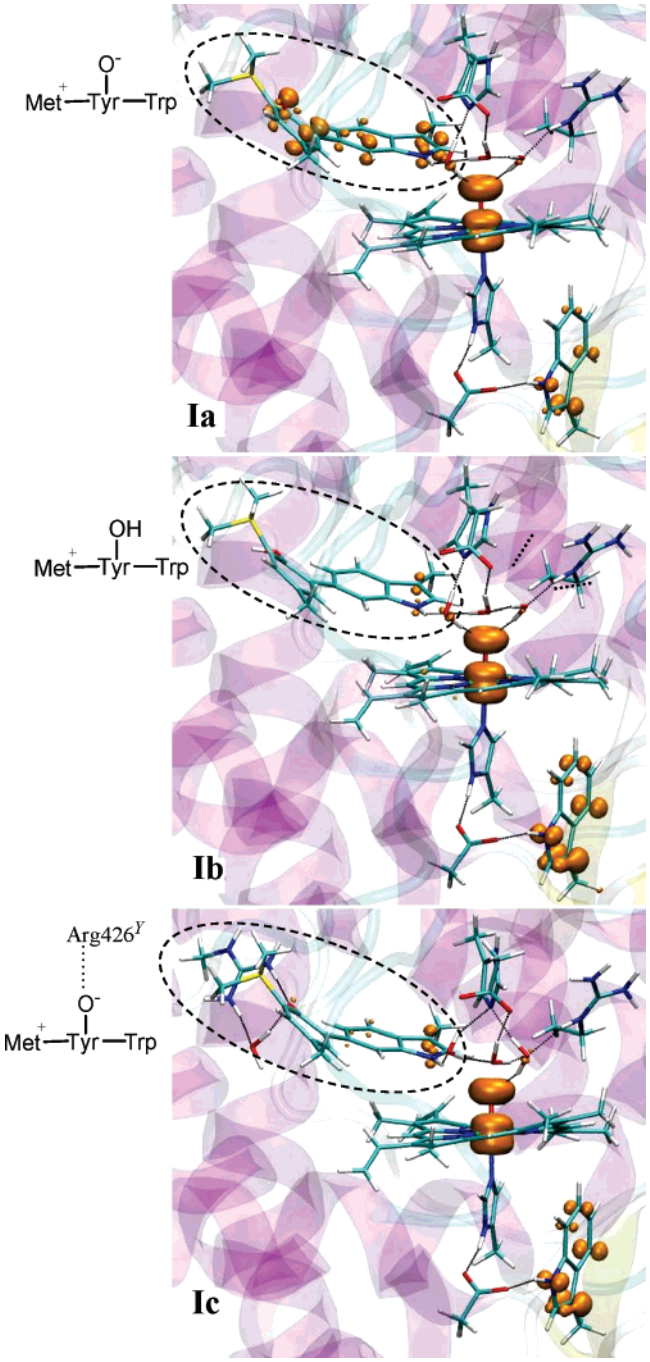

Figure 3. Spin density distribution of Cpd I (oxoferryl forms). The isodensity surface at 0.005 e Å^{-3} is plotted in orange. The atoms treated at the QM level in our QM/MM calculations are represented by sticks, while the protein frame is displayed as a transparent cartoon. (Top) Arg426 (not shown) is in the *R* position, and Tyr238 is unprotonated (model **Ia**). (Center) Arg426 (not shown) is in the *R* position, and Tyr238 is protonated (**Ib**). (Bottom) Arg426 is in the *Y* position, and Tyr238 is unprotonated (**Ic**).

that a porphyrin radical species is not stable. This result is independent of the protonation state of the oxoferryl bond (Tables 6 and 4S). The spin density delocalizes into the adduct and Trp330. When the adduct is unprotonated (**Ia**), the unpaired electron localizes mainly on the adduct (0.7 e), but when the adduct is protonated (**Ib**), the unpaired electron localizes mainly on Trp330 (0.6 e). Therefore, the amount of unpaired spins in these residues depends on the protonation state of the adduct. The values obtained are consistent with the IPs calculated for the isolated adduct (the unprotonated adduct is a better electron

Table 6. Distribution of the Three Unpaired Electrons in Cpd I (Oxoferryl Form)[a]

		Ia	Ib	Ic
FeO		2.0	2.2	2.2
adduct		0.7	0.1	0.3
	Met264	0.0	0.0	0.0
	Tyr238	0.4	0.0	0.1
	Trp111	0.3	0.1	0.2
Porph		0.0	0.1	0.0
Trp330		0.3	0.6	0.5

[a] The results for the hydroxoferryl forms are reported in the Supporting Information (Table 3S).

donor than the protonated one). The spin-density distribution of **Ic** is close to that of **Ib** (Table 6 and 4S), showing predominantly a Trp330 radical. This is consistent with the IPs computed for the various configurations of the adduct, in particular that the IPs of Met^{+}-Tyr(O^{-})-Trp:$Arg426^{Y}$ (191 kcal/mol) and Met^{+}-Tyr(OH)-Trp (218 kcal/mol) are significantly higher than the IP of Met^{+}-Tyr(O^{-})-Trp (132 kcal/mol).

Additional calculations were performed to investigate the effect of the cross-link between Trp111 and Tyr238 in the electronic structure of **Ia**. When only Trp111 is included in the QM region (model **A** and **C**), the amount of spin density previously present on Tyr238 is now on Trp330 and on the porphyrin (Table 7). Therefore, when the structure is forced toward a CcP active site, the spin-density distribution also displays CcP features[12] (APX is structurally similar to CcP at the active site but displays a classical porphyrin cation radical Cpd I[12]). Similar calculations were performed to investigate the effect of Asp141, a residue not present in CcP. The same spin-density distribution is observed when treating the Asp141 side chain at the MM (model **B**) or QM level (**Ia**), indicating that the role of Asp141 on the electronic properties of Cpd I is mainly electrostatic. Asp141 acts to stabilize the radical on the distal side of the heme, because in models **B′** and **C′**, with the Asp charges switched off, there is a shift of the spin density toward Trp330 compared to models **B** and **C**, respectively (Table 7). **C′** is the model that best resembles the CcP active site, and it is also the one showing the largest amount of spin density on the proximal Trp (0.6 e). The amount of spin density on the proximal Trp is smaller than what was found in QM/MM calculations on CcP Cpd I, although in this study the distal Trp was not included in the QM region.[46] Models **D** and **D′** highlight the importance of Met264 on the spin distribution on the adduct: the positive charge of Met264 reduces the electron donor capability of the adduct, resulting in a smaller amount of unpaired spin on the adduct.

The largest models we considered are **E** and **F**. **E** comprises the heme propionates and their H-bonding partners (Ser324, His285, Asp98, and a water molecule, Figure 4S) into the QM region. Model **F** includes Trp95 into the QM region. Trp95 is a conserved residue among KatGs and a radical site in *Synechocystis* PCC6803, SyKatG, according to EPR experiments.[77] It turns out that the spin-density distribution in models **E** and **F** is very similar to models **I** (Table 4S); i.e. no radical character is observed either on the heme propionates or on Trp95.

When protein thermal fluctuations are accounted for, the overall picture is maintained, although variations of the spin-density distribution are observed (see SI, Table S7), especially for the models showing a Trp330 radical (**Ib** and **Ic**). In fact, for model **Ia** a large fraction of the spin density is observed on the adduct in all MD snaphots analyzed. On the contrary, the amount of spin density on the adduct is small in any of the MD snapshots of model **Ib**. These are the same features observed by analysis of the optimized structures. The active site of BpKatG was observed to be the most rigid part of the protein in MD simulations and X-ray studies (see Supporting Information, section 5S). However, small structural fluctuatiuons affect the spin-density distribution. Among the many geometrical parameters that may play a role in modulating the spin-density distribution, we mention the number of water molecules H-bonding to the FeO group, the strength (i.e., the length) of the interaction between Trp330 and Asp389, and that between Tyr238 and Arg426. However, due to the limited number of conformations considered, no clear correlation could be inferred.

In the X-ray structure of putative Cpd I, Arg426 was observed only in conformation *R*, at any pH. Thus, the pH-dependent equilibrium between the *R* and *Y* conformations of Arg426 observed in the native enzyme is completely shifted toward the *R* conformation in Cpd I. In order to rationalize these findings, knowing the energy difference between models **Ia** and **Ic** would be desirable. Unfortunately, since the two models differ for the QM/MM partitions and for protein and solvent conformation, their energies are not comparable. Thus, we turned to a simplified model intended to mimic the $R \rightarrow Y$ conformational change and the consequent electronic rearrangement observed in QM/MM calculations of models **Ia** and **Ic** (Figure 3 and Table 6). Specifically, we calculated the free energy change of the following reaction (**Ia** → **Ic**):

$$Met^{+}\text{-}Tyr(O^{\bullet})\text{-}Trp\cdots Arg426^{R} + Trp330 \rightarrow Met^{+}\text{-}Tyr(O^{-})\text{-}Trp\cdots Arg426^{Y} + Trp330^{+\bullet}$$

Models for Met-Tyr($O^{\bullet}$)-Trp···$Arg426^{R}$ and Met^{+}-Tyr(O^{-})-Trp···$Arg426^{Y}$ are as in Figure 5S (the appropriate number of electrons was considered) and Trp330 was modeled as an indole molecule. It turned out that the above reaction is unfavorable as it is written, with reactants more stable by 10.8 kcal/mol in water solution ($\epsilon = 80$) and by 3.2 kcal/mol in a low dielectric medium ($\epsilon = 4$). The unfavorable energetics would agree with the experimental observation of Arg426 being 100% *R* in the Cpd I crystal structure even at high pH.[37]

3.3. The Cpd II Active Site. One-electron reduction of the active site of Cpd I, either by reactions 2 or 4, leads to the formation of a Cpd II active site. Figure 2S shows the optimized geometry of the Cpd II active site, while Figure 3S shows the corresponding spin-density distribution. Our analysis of Cpd II is based on the hydroxoferryl forms of Cpd II, because this is the most realistic configuration based on recent studies.[9,11,41,42] Table 8 shows that the spin density delocalized in the adduct and/or Trp330 is taken at the expense of the Fe−OH fragment. The shape of the spin-density distribution at the iron (Figure 3S) shows that only one of the iron d_{π} orbitals (d_{xz} or d_{yz}) is singly occupied unlike the situation in Cpd I (Figure 3). Therefore, the oxidation state of the iron atom in KatG-Cpd II is better described as Fe^{III}, rather than Fe^{IV} as in the classical Cpd II state of monofunctional catalases.[11] A similar scenario was recently reported for HRP Cpd II, where it was found that

(77) Jakopitsch, C.; Obinger, C.; Un, S.; Ivancich, A. *J. Inorg. Biochem.* **2006**, *100*, 1091−1099.

Table 7. Comparison of Different Models and Setups Starting from **Ia**

	Ia	**A** *Tyr238-Met 264 in MM*	**B** *Asp141 in MM*	**C** *(A+B)*	**D** *Met264 in MM*	**B′** *≈ D141G*	**C′** *(A + B′) ≈ CcP*	**D′** *≈ M264G*
FeO	2.0	2.1	2.0	2.1	2.0	2.0	2.0	2.0
Adduct	0.7	0.3	0.7	0.3	0.9	0.6	0.3	1.0
Porph	0.0	0.2	0.0	0.2	0.0	0.0	0.1	0.0
Trp330	0.3	0.4	0.3	0.4	0.1	0.4	0.6	0.0

Table 8. Distribution of the Two Unpaired Electrons in Cpd II (Hydroxoferryl Form)

		IIa		**IIb**
Fe−OH		1.2		1.5
Adduct		0.6		0.0
	Met264	*0.0*		*0.0*
	Tyr238	*0.4*		*0.0*
	Trp111	*0.2*		*0.0*
Porph		0.1		0.1
Trp330		0.1		0.4

the most stable hydroxoferryl form of HRP is a $Por^{+\bullet}Fe^{III}OH$ species.[45] The calculations reported here display a similar Fe^{III} oxidation state, with the electron-reducing Fe^{IV} coming either from Trp330 or from the covalent adduct, depending on the protonation state of Tyr238 (Figure 3S and Table 8). KatG differs from HRP in that it possesses more easily ionizable residues on the proximal and distal side of the heme: Trp330 (a Phe in HRP), Tyr238, and Trp111 (only a Phe in HRP). It was also recently proposed that the spectroscopic features of MtKatG[14] Cpd II may be explained as a $(KatG^{\bullet})Fe^{III}-X$ ($X = OH^-$ or H_2O) structure, whereas MtKatG(Y229F) (Y238F in BpKatG numbering) is the typical oxoferryl species. Nevertheless, there is no evidence of a protein-based radical in KatG Cpd II from Mössbauer or EPR measurements.

4. Discussion

The basic peroxidase core of KatGs consists of the His112/Arg108/Trp111 (BpKatG numbering throughout) triad on the distal side, together with His279, Asp389, and Trp330 on the proximal side (Figure 1). Supplementing the core with a small number of additional residues, including Asp141, the unusual Met264-Tyr238-Trp111 covalently linked adduct and Arg426, converts the enzyme into a moderately efficient catalase. In particular, both the integrity of the adduct and the presence of Arg426 are necessary for catalatic activity.[14,15,25,27−29,37,78] Arg426 participates in a pH-sensitive interaction with Tyr238 which lowers the apparent pK_a of Tyr238 to 6.5 (inferred from crystallographic studies[37,38]) from the expected pK_a of about 10 for a normal Tyr. Understanding the role of the Met264-Tyr238-Trp111 adduct (Figure 1) in the reaction mechanism is a major topic in biochemical studies of KatGs.[14,16,25,38]

The first step toward elucidating the enzyme reaction mechanism is to characterize the structure and electronic structure of the reaction intermediates. The crystal structures of KatG Cpd I[37], obtained upon reaction of the enzyme with organic peroxides, show that Arg426 adopts fully the *R* conformation (i.e., not interacting with the adduct), while mixtures of both *R* and *Y* conformations are found in the native enzyme, the relative proportions being pH dependent.[38] Interestingly, recent spectroscopic investigations of the reaction of KatG with H_2O_2 detected different species, depending on the pH.[17] These observations prompted us to investigate by quantum mechanical methods the electronic properties of the Met^+-Tyr-Trp adduct and the KatG reaction intermediates for different protonation states of Tyr238 and its different association states with Arg426.

The classical catalase and peroxidase Cpd I contains the heme oxidized to the oxoferryl state ($Fe^{IV} = O$) and a second oxidizing equivalent stored on the porphyrin.[12] Our QM/MM calculations show that when only the heme prosthetic group is included in the QM region, the classical $Fe^{IV} = O-Por^{+\bullet}$ is observed (Table 5S). However, as soon as the neighboring residues are included in the QM region, the porphyrin radical tends to be reduced. When only Trp330 is in the QM region, the radical character is shared between the Por and the indole side chain. When only the distal adduct is included in the QM region, the radical localizes onto the adduct when this is deprotonated but remains on the porphyrin if the adduct is protonated. Including both the distal adduct and the proximal Trp into the QM region reveals that little spin density is observed on the porphyrin. The unpaired spin localizes mainly on the unprotonated adduct when Arg426 is in the *R* conformation [Met^+-$Tyr(O^-)$-Trp:Arg^R] (**Ia**). In contrast, the unpaired electron localizes mainly on Trp330 either when the adduct is protonated [Met^+-Tyr(OH)-Trp:Arg^R] (**Ib**) or when Arg426 interacts with it [Met^+-$Tyr(O^-)$-Trp:Arg^Y] (**Ic**). In either of these two configurations (**Ib** or **Ic**), the electron distribution resembles that of CcP. Similar results are obtained when both Met264-Tyr238 residues are not treated quantum mechanically (i.e., the electron density is not allowed to delocalize through most of the adduct) (Table 7).

The overall picture is not affected by the conformational fluctuations of the protein, although variations of the spin distribution are observed. In fact, a large fraction of the spin density is observed on the adduct in all conformations analyzed for model **Ia**. On the contrary, the amount of spin density on the adduct is small in any of the MD snapshots of model **Ib**. In model **Ib**, conformational fluctuations may lead to the delocalization of spin density onto the porphyrin, resembling the classical porphyrin cation radical form of Cpd I. As noted in the following, KatGs differ from both CcP and APX in terms of the interactions that account for the stabilization of the proximal Trp radical with respect to the porphyrin radical. Thus, although the magnitude of the fluctuations are determined by the force field used, it seems reasonable that small structural fluctuations may shift spin density from one site to the other.

In QM/MM calculations, the possibility to observe protein-based radicals is limited to the region treated at the QM level. Protein-based radical species have been observed in several catalases and peroxidases and may possibly be directly involved in the enzymatic reaction.[17] In KatGs, the intermediates formed during the reaction with peroxyacetic acid (PAA) in the absence of electron donor(s) have been characterized by EPR spectros-

(78) Ghiladi, R. A.; Medzihradszky, K. F.; Rusnak, F. M.; de Montellano, P. R. *J. Am. Chem. Soc.* **2005**, *127*, 13428−13442.

copy. It was shown that the *Synechocystis* enzyme (SyKatG) forms the typical oxoferryl porphyrin radical and two subsequent protein-based radicals (Trp106 and a Tyr radical of unknown location).[77] In contrast, the *M. tuberculosis* enzyme (MtKatG) appears to form only a tyrosyl radical,[79] the radical site (Tyr353) being a nonconserved Tyr residue among KatGs.[80] A recent study using rapid freeze/quench EPR concludes that Tyr229 (equivalent to Tyr238 in BpKatG) is the first radical site in MtKatG.[81] Thus, the adduct radical could exist but would have a lifetime too short to observe under the experimental conditions employed. The presence of some phenolate side chain would account for the Tyr radicals observed in MtKatG and SyKatG. Similarly, the protein frame may stabilize Trp radicals, as in lignin peroxidase.[82,83] Nevertheless, radical chemistry is proposed to be involved in the formation of the Met264-Tyr238-Trp111 covalent adduct.[14] Furthermore, formation of a distal side Trp radical was recently observed on exposure of APX to H_2O_2 under noncatalytic conditions.[84]

A model to rationalize the chameleon nature of Cpd I, proposed by de Visser and co-workers,[43] turns out to be suitable for the present discussion. The model relies on a valence bond description of the electronic structure of Cpd I, expressed as the combination of different forms. Four forms are of interest here:

$$|a\rangle:\ \text{Trp330-Add-aa-Fe}^{IV}\text{=O}-\text{Porph}^{+\bullet}$$

$$|b\rangle:\ \text{Trp330}^{+\bullet}\text{-Add-aa-Fe}^{IV}\text{=O}-\text{Porph}$$

$$|c\rangle:\ \text{Trp330-Add}^{+\bullet}\text{-aa-Fe}^{IV}\text{=O}-\text{Porph}$$

$$|d\rangle:\ \text{Trp330-Add-aa}^{+\bullet}\text{-Fe}^{IV}\text{=O}-\text{Porph}$$

where Add stands for the Met264-Tyr238-Trp111 adduct and aa is a protein-specific residue, usually a Tyr or Trp residue. The mixing of the different forms depends on the energy gaps between them, which are given by the difference between the IP of the donor group and the electron affinity of the acceptor, their orbital overlap, and the difference in electrostatic interaction energy in the two forms.[43]

The model was originally introduced to clarify the difference between Cpd I of CcP and HRP,[43] suggesting that the protein frame stabilizes the $|a\rangle$ form in HRP and the $|b\rangle$ form in CcP. In the gas phase, forms $|a\rangle$ and $|b\rangle$ are degenerate.[85] As shown by Poulos in a series of studies on CcP,[86−88] relatively minor variations in the protein environment can shift the radical cationic species around. CcP and APX, structurally very similar (33% sequence identity), especially in the vicinity of the heme group (the His-Asp-Trp triad on the proximal side), display different Cpd I electronic structures ($|b\rangle$-like in CcP and $|a\rangle$-like in APX[23]). Continuum electrostatics calculations showed that in CcP the protein frame stabilizes a proximal cation radical species,[88] while no such stabilization was found in APX. A study by Jensen and co-workers,[89] based on the protein dipoles Langevin dipoles model, concluded that several factors contribute to stabilization of the proximal Trp radical cation in CcP with respect to APX. Similar conclusions were achieved by Harvey et al. from QM/MM studies.[46] Among the contributions that account for the different electronic structure in CcP and APX are the presence of a potassium ion 8 Å from the proximal Trp in APX (destabilizing the Trp cation radical) and the contribution of Met230 in CcP (stabilizing the cation radical Trp, substituted by Leu203 in APX). In KatG X-ray structures, no cations were detected near the proximal pocket, while CcP Met230 is replaced by Thr384 in BpKatG. Our QM/MM calculations indicate that in the optimized models of BpKatG, $|b\rangle$ is favored over $|a\rangle$. However, protein thermal fluctuations may favor one form with respect to the other.

Further migration of the radical to more distant residues ($|d\rangle$ form, also known as Cpd I*), as observed in MtKatG and SyKatG, cannot be ruled out on the basis of our calculations. The largest models we considered comprised the heme propionates (model E) or Trp95, equivalent to Trp106 in MtKatG, (model F) in the QM region, and no spin density was observed on these groups (Table 3S and Figure 4S).

From the above discussion we conclude that the energy levels of forms $|a\rangle$, $|b\rangle$, and $|d\rangle$ are determined by the protein environment. What appears to be characteristic of KatGs is the possibility of switching the electronic state, depending on the pH. Indeed, the energy level of form $|c\rangle$ is modulated by the pH and the association with Arg426. The unprotonated adduct [Met^+-Tyr(O^-)-Trp] is a better electron donor (lower IP) than the protonated one [Met^+-Tyr(OH)-Trp], and its donor ability is reduced when Arg426 is associated with it (Table 4). The IP of [Met^+-Tyr(O^-)-Trp] is higher than that of phenolate and indolide, but lower than that of the neutral species, phenol and indole. Indeed, QM/MM calculations show that when the adduct is deprotonated, form $|c\rangle$ predominates. After protonation of Tyr238 or its association with Arg426, the energy of $|c\rangle$ is increased, and the radical moves to a site determined by the protein frame. Further studies are needed to ascertain whether and how this feature may be related to the bifunctionality of the enzyme. In the following we put forward some simple considerations.

Figure 4 shows our proposed reaction scheme, along with the location of the computed species. The porphyrin-cation-radical form of Cpd I has been included since it has been observed experimentally in SyKatG.[7,77] Interconversion between the different forms should be possible, ensuring that the enzyme does not get blocked in a given intermediate state if the competent substrate is missing.[17] In view of the experimental and theoretical data available, several forms of Cpd I are possibly relevant for catalysis. Unfortunately, a possible relation of these Cpd I forms with the results of UV−visible spectroscopic experiments in KatGs[17] cannot be drawn, since differences in radical sites cannot be elucidated from UV−visible

(79) Chouchane, S.; Lippai, I.; Magliozzo, R. S. *Biochemistry* **2000**, *39*, 9975−9983.
(80) Yu, S. W.; Girotto, S.; Zhao, X. B.; Magliozzo, R. S. *J. Biol. Chem.* **2003**, *278*, 44121−44127.
(81) Ranguelova, K.; Girotto, S.; Gerfen, G. J.; Yu, S. W.; Suarez, J.; Metlitsky, L.; Magliozzo, R. S. *J. Biol. Chem.* **2007**, *282*, 6255−6264.
(82) Blodig, W.; Smith, A. T.; Winterhalter, K.; Piontek, K. *Arch. Biochem. Biophys.* **1999**, *370*, 86−92.
(83) Blodig, W.; Doyle, W.; Smith, A. T.; Winterhalter, K.; Piontek, K. *J. Inorg. Biochem.* **1999**, *74*, 266.
(84) Pipirou, Z.; Bottrill, A. R.; Metcalfe, C. M.; Mistry, S. C.; Badyal, S. K.; Rawlings, B. J.; Raven, E. L. *Biochemistry* **2007**, *46*, 2174−2180.
(85) Wirstam, M.; Blomberg, M. R. A.; Siegbahn, P. E. M. *J. Am. Chem. Soc.* **1999**, *121*, 10178−10185.
(86) Barrows, T. P.; Bhaskar, B.; Poulos, T. L. *Biochemistry* **2004**, *43*, 8826−8834.
(87) Bhaskar, B.; Bonagura, C. A.; Li, H. Y.; Poulos, T. L. *Biochemistry* **2002**, *41*, 2684−2693.
(88) Bonagura, C. A.; Sundaramoorthy, M.; Pappa, H. S.; Patterson, W. R.; Poulos, T. L. *Biochemistry* **1996**, *35*, 6107−6115.
(89) Jensen, G. M.; Bunte, S. W.; Warshel, A.; Goodin, D. B. *J. Phys. Chem. B* **1998**, *102*, 8221−8228.

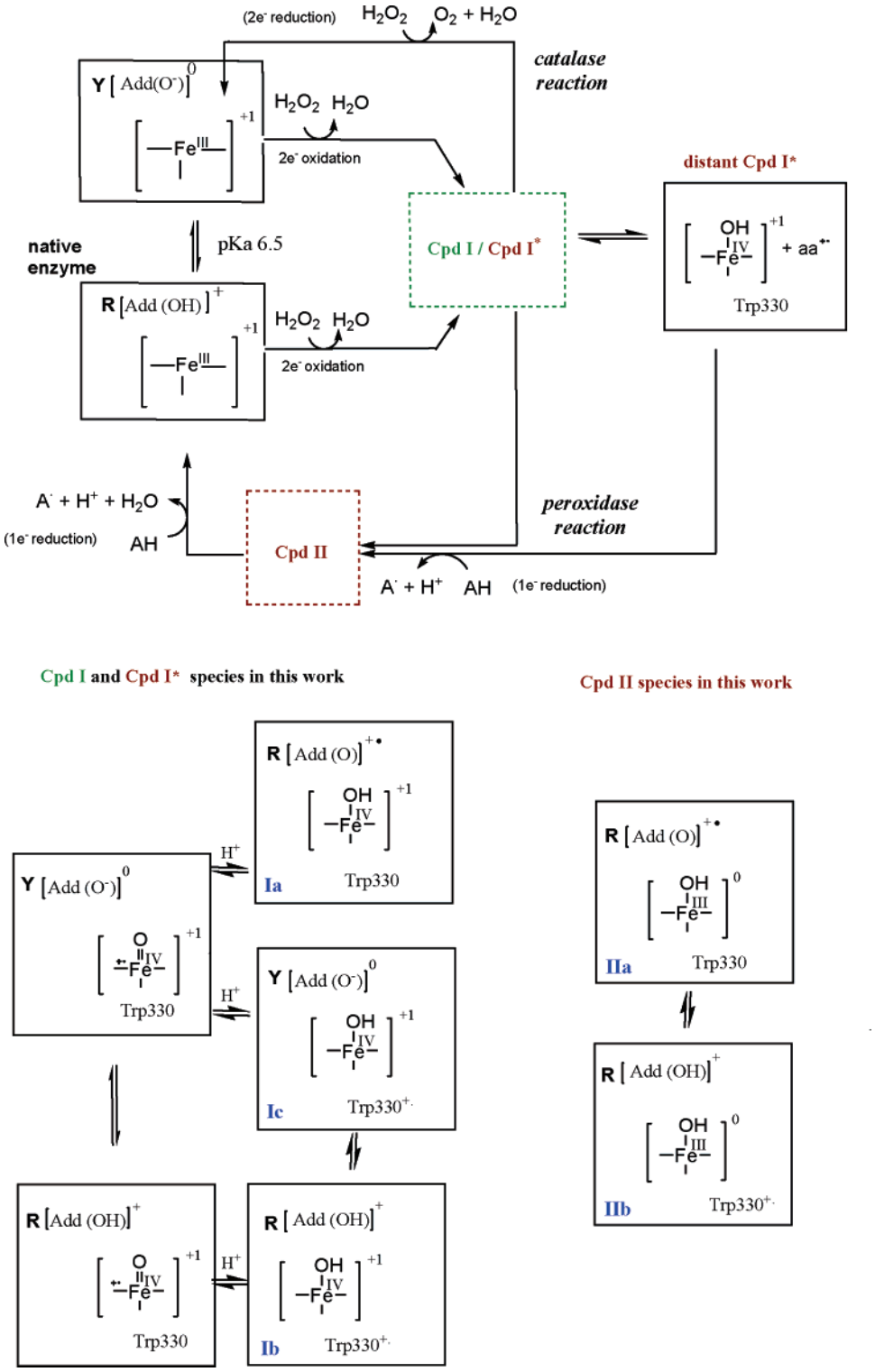

Figure 4. General scheme showing the possible transformations of KatG upon reaction with H_2O_2 and exogenous electron donors. The total charge of the central heme complex and the adduct is indicated in brackets. The computed species are identified by blue labels. The following notation is used: Add = Met^+-Tyr-Trp adduct, **R** = $Arg426^R$, **Y** = $Arg426^Y$, $aa^{+\bullet}$ = protein radical, AH = endogenous electron donor.

spectroscopic techniques alone. The reduction of a catalase Cpd I has usually been understood to imply reduction of the porphyrin cation radical, whereas the reduction of a peroxidase Cpd I may involve reduction of a protein radical some distance from the heme. Therefore, if protein radicals are to be intermediates in the catalase reaction they should be in close proximity to the heme to allow their rapid reduction by H_2O_2 binding in the heme cavity. If sufficient H_2O_2 is present to promote catalatic reduction of Cpd I ($K_m \approx 4$ mM), the radical remains in close proximity to the heme, whereas a negligible catalatic reaction, arising from low levels of H_2O_2 or the involvement of an organic peroxide, allows the radical to move further into the protein. According to this criterion, the porphyrin radical and species **Ia**, **Ib**, and **Ic** all store two oxidation equivalents within the heme cavity, which would seem appropriate for the catalatic reaction, while the more distant Cpd

I* species may undergo two sequential one-electron reductions. Within this scenario, the presence of the adduct either alters the redox potential of Cpd I, making it more suitable for the reaction with H_2O_2, or hinders the formation of the distant Cpd I*.

As an alternative criterion, we may consider the location of a radical site with respect to the heme plane (distal vs proximal). Indeed, a species like **Ia**, with the radical on the distal side of the heme, has not been reported so far for peroxidases (only very recently, formation of a distal side Trp radical was observed on exposure of APX to H_2O_2 under noncatalytic conditions.[84]), whereas **Ib** (and **Ic)** are similar to Cpd I in CcP, a monofunctional peroxidase. Therefore, **Ia** and the oxoferryl-porphyrin radical form, storing two oxidation equivalents on the heme/or its distal side, might be more appropriate for the catalatic reaction, whereas **Ib**, **Ic**, and the distant Cpd I* might be associated to the peroxidatic reaction.

In summary, our calculations predict a family of Cpd I intermediates of KatGs, having similar protein and heme structures, but very different electronic structures. The Cpd I species formed at low pH, **Ib** or [Met^+-Tyr(OH)-Trp:Arg^R], holds the radical on the proximal Trp, similar to CcP, whereas the Cpd I species formed at high pH, **Ia** or [Met^+-Tyr(O^-)-Trp:Arg^R], holds the radical on the adduct with the implication of an equilibrium mixture of the two species at intermediate pH's.

Abbreviations: KatGs, catalase-peroxidases; Bp, *Burkholderia pseudomallei*; Mt, *Mycobacterium tuberculosis*; Hm, *Haloarcula marismortui*; Sy, *Synechocystis* PCC6803; CPMD, Car—Parrinello molecular dynamics; QM, quantum mechanics; MM, molecular mechanics; MD, molecular dynamics; CP, Car—Parrinello; DFT, Density Functional Theory.

Acknowledgment. This work was supported by Grants 2005SGR-00036 from the *Generalitat de Catalunya (GENCAT*), FIS2005-00655, BFU2004-06377-C02-02 from the *Ministerio de Educación y Cencia* (MEC), Spain, by Grant OGP9600 from the Natural Sciences and Engineering Research Council of Canada (to P.C.L.), and by the Canadian Research Chair Program (to P.C.L). Financial support from the Juan de la Cierva program of MEC (to P.V.), the I3P program of the Spanish Research Council (to X.C.), and the F.I. fellowship program of the GENCAT (to M.A.-P.) was provided. The authors thankfully acknowledge the computer resources, technical expertise and assistance provided by the Barcelona Supercomputing Center - Centro Nacional de Supercomputación.

Supporting Information Available: Structures of the active site in the different forms of Cpd I and Cpd II analyzed; spin density distribution of Cpd I for different QM/MM partitions and spin states; spin density distribution of Cpd II; details of pK_a and binding energy calculations; computational details and analysis of classical MD simulations. This material is available free of charge via the Internet at http://pubs.acs.org.

JA072245I